Structural transition of the tetrahedral metal cluster: nuclear magnetic resonance study of GaV_4S_8

2005 J. Phys.: Condens. Matter 17 6015

(http://iopscience.iop.org/0953-8984/17/38/007)

INSTITUTE OF PHYSICS PUBLISHING JOURNAL OF PHYSICS: CONDENSED MATTER

J. Phys.: Condens. Matter **17** (2005) 6015–6024 doi:10.1088/0953-8984/17/38/007

Structural transition of the tetrahedral metal cluster: nuclear magnetic resonance study of GaV_4S_8

H Nakamura[1], **H Chudo**[2] **and M Shiga**

Department of Materials Science and Engineering, Kyoto University, Kyoto 606-8501, Japan

E-mail: naka6ra@sci.u-hyogo.ac.jp

Received 18 May 2005, in final form 19 August 2005
Published 9 September 2005
Online at stacks.iop.org/JPhysCM/17/6015

Abstract

The small rhombohedral distortion (at $T_S \simeq 44$ K), observed for the V_4 tetrahedral cluster involved in the cubic compound GaV_4S_8, has been investigated by means of nuclear magnetic resonance (NMR). ^{51}V NMR experiments successfully monitored the considerable change in the electronic state inside the cluster. The isotropic term of ^{51}V hyperfine coupling is reduced markedly, and instead large anisotropy appears below T_S. The ^{51}V nuclear spin–lattice relaxation rate is reduced markedly below T_S, suggesting a reduction of the density of states in the spin excitation spectrum. The structural transition can be interpreted as the Jahn–Teller instability resulting from the orbital degeneracy of the highest occupied 3d cluster orbitals in the V_4 tetrahedral cluster. The drastic change in the NMR quantities at T_S is explained as a transition from the electron occupation in nearly spherical degenerate orbitals to that in a strongly asymmetric non-degenerate orbital.

1. Introduction

In this paper, we report a nuclear magnetic resonance (NMR) study of *magnetic metal* (nano-) clusters in the paramagnetic state. The *metal* cluster is the assembly of the small number of transition-metal atoms in which intracluster atoms share common d electrons to form a molecular-orbital-like cluster orbital state, i.e. metallic bonds within the cluster. The *magnetic* cluster means that at least one unpaired spin is involved in the cluster, implying that each cluster behaves like a localized moment. In the present study, we particularly treat a four-atom tetrahedral cluster with high structural symmetry, where the degeneracy of d electron cluster orbitals is expected.

[1] Author to whom any correspondence should be addressed. Present address: Graduate School of Material Science, University of Hyogo, Kamigori, Ako-gun, Hyogo 678-1297, Japan.
[2] Present address: Department of Chemistry, Graduate School of Science, Kyoto University, Kyoto 606-8502, Japan.

0953-8984/05/386015+10$30.00

Motivation of the present study is twofold. A lot of NMR studies have already been reported for both typical localized-moment and metallic magnets. However, few works can be found for such magnetic metal clusters. The study of typical magnetic metal clusters, which may have intermediate characteristics between insulator and metal, should be helpful in understanding the system being at the vicinity of the metal–insulator instability in the strongly correlated electron system, which attracts much attention as one of essential problems in solid-state physics [1]. The other motivation is related to effects of the geometric frustration in the pyrochlore lattice, an infinite lattice of corner-shared tetrahedra. Unusual magnetic properties observed for a number of pyrochlore compounds (including spinel and Laves phases) attract much attention of many researchers [2]. A number of pyrochlore compounds have been known to show structural instability. Here we should note that an isolated tetrahedron is already the smallest unit of the three-dimensional frustrated system, and that the electronic-state degeneracy inherent to a single tetrahedron may result in anomalous properties. Hence, to separate the anomalies originating in the coherence of the infinite lattice from those of the single tetrahedron, the study of the tetrahedral cluster may be of importance.

Tetrahedral metal clusters are found among intermetallic compounds as well as molecular crystals [3]. A compound with the cubic $GaMo_4S_8$-type crystal structure, which includes the *cubane*-type cluster, is one of the candidates [4]. In this study, we select GaV_4S_8 with vanadium tetrahedral clusters [5], which shows a structural transition in the paramagnetic state, and report its NMR results both above and below the structural transition. The results obtained are explained in terms of cluster orbital schemes discussed by Pocha *et al* [6]. Results in the magnetically ordered state will be reported elsewhere.

2. Structure and magnetism of GaV_4S_8

GaV_4S_8 forms the $GaMo_4S_8$-type crystal structure (space group $F\bar{4}3m$). The *defect spinel* structure is often referred to in explaining this structure [7]. In AB_4X_8 (=$A_{0.5}B_2X_4$), A atoms and vacancies order in 1:1 ratio on the A site of the normal spinel lattice AB_2X_4. As a result, B atoms, which form the corner-shared tetrahedral lattice, approach the vacancy site and the B–B interatomic distances separate to long and short to form tetrahedral clusters. Due to the symmetry lowering, the space group $Fd\bar{3}m$ of AB_2X_4 changes to $F\bar{4}3m$ in AB_4X_8. The B site changes from 16d at $(\frac{5}{8}\frac{5}{8}\frac{5}{8})$ in $Fd\bar{3}m$ to 16e at (xxx) with $x < \frac{5}{8}$ in $F\bar{4}3m$.

As magnetic compounds, 3d transition-metal compounds, GaV_4S_8, GaV_4Se_8, etc, and 4d compounds, $GaMo_4S_8$, $AlMo_4S_8$, etc, have been known [4]. In these compounds, the intracluster atomic distance is close to that of pure metal, resulting in metallic bonds inside the cluster, while the intercluster distance is sufficiently larger, leading to semiconducting features of the whole lattice. Crystallographic parameters of GaV_4S_8 are found in some literatures [4–6]. The lattice parameter at 295 K was reported to be $a = 9.666$ Å [6]. The intracluster and intercluster V–V distances in GaV_4S_8 are 2.896 and 3.936 Å, respectively. Hopping conduction among clusters has been argued in detail [8–11]. The charge gap was estimated to be $E_g = 0.1$–0.15 eV from conductivity measurements [6, 8].

In considering the electronic structure, it is more reasonable to treat this structure as an NaCl-type weakly coupled network (see figure 1(c)) of cubane-type cluster ions, $(B_4X_4)^{n+}$ (figure 1(a)), and tetrahedral ions, $(AX_4)^{n-}$ (figure 1(b)), rather than the defect spinel picture. This consideration is consistent with electronic structure calculations [6, 12, 13]. In the B_4X_4 cubane-type cluster, two regular tetrahedra of B_4 and X_4 with slightly different sizes (X_4 is generally larger) are interpenetrated to form a distorted cube. Among the $GaMo_4S_8$-type compounds, $GaMo_4S_8$ has most extensively been investigated because ferromagnetism was found for the first time among 4d transition-metal materials [14]. The magnetic and structural properties of GaV_4S_8 are quite similar to those of $GaMo_4S_8$. From formal valence, it is

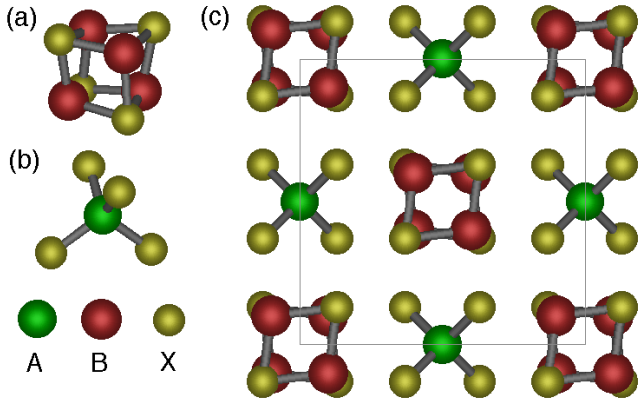

Figure 1. (a) A $(B_4X_4)^{n+}$ cubane-type cluster, (b) an $(AX_4)^{n-}$ tetrahedral cluster, and (c) the $GaMo_4S_8$-type structure (projected on the (001) plane) as an NaCl-type network of $(B_4X_4)^{n+}$ and $(AX_4)^{n-}$ ions. Thin lines represent the crystallographic unit cell.

(This figure is in colour only in the electronic version)

suggested that $(V_4S_4)^{5-}$ in GaV_4S_8 has seven 3d electrons per V_4 cluster. Since Curie–Weiss behaviour, corresponding roughly to $S = \frac{1}{2}$, has been observed [5], it was suggested that one of the d-based orbitals in the cluster is singly occupied. A small rhombohedral crystal distortion to the space group $R3m$ has been found at $T_S = 38$–46 K [4, 6] like the case of $GaMo_4S_8$ [15]. As a result of the structural transition, the V site separates into two inequivalent sites with the population ratio of 1:3. The rhombohedral lattice parameters, $a_{rh} = 6.384$ Å and $\alpha_{rh} = 59.66°$ [6], imply that the V tetrahedron expands slightly along the trigonal axis and shrinks at the triangle base perpendicular to the trigonal axis. This tendency is opposite to the case of $GaMo_4S_8$. This difference was explained in terms of the cluster orbital schemes [6]. The magnetic ground state is ferromagnetic with $T_C = 10$–13 K [5, 6]. The saturation moment is in rough agreement with that expected for $S = \frac{1}{2}$ per cluster [6]. Microscopic magnetic experiments, which can discriminate intracluster and intercluster interactions, have not been reported.

3. Experimental procedures

A polycrystalline sample of GaV_4S_8 was prepared by solid-state reactions from a mixture of pure elements in powder form in an evacuated quartz tube. The purity of starting materials, Ga, V, and S, was 99.99, 99.9 and 99.9999%, respectively. The mixture was kept for 2 days at 950 °C. The product was crushed once, pelletized and heated again in an evacuated quartz tube at 950 °C for 2 days. Results of x-ray analysis at 290 and 7 K are practically the same as those reported by Pocha *et al* [6]. The susceptibility was measured using a SQUID magnetometer (Quantum Design, MPMS-5). NMR was measured by the spin-echo method using a pulsed spectrometer. The nuclear spin–lattice relaxation time T_1 was measured by the saturation recovery method. For ^{51}V (nuclear spin $I = \frac{7}{2}$), we used 11.983 T/μ_B as the gyromagnetic ratio.

4. Experimental results

4.1. Susceptibility

Figure 2 shows temperature dependences of magnetization, M ($T < T_C$), and inverse susceptibility, $1/\chi$ ($T > T_C$), measured at fields of 0.01 and 1 T, respectively. The Curie

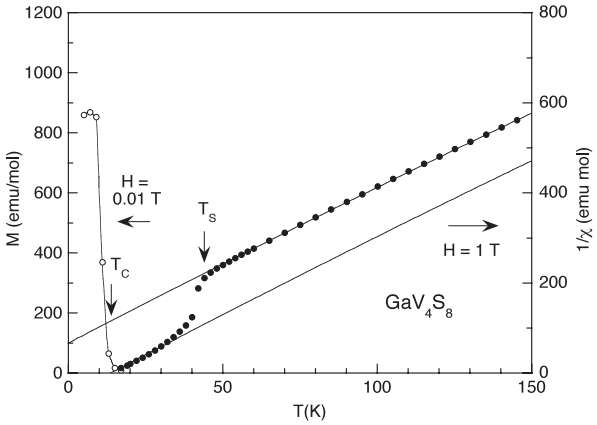

Figure 2. Temperature dependences of magnetization ($T < T_C$) and inverse susceptibility ($T > T_C$) for GaV_4S_8. The low-temperature magnetization was measured at 0.01 T, and the paramagnetic susceptibility at 1 T. Straight lines indicate the Curie–Weiss fits with the same effective paramagnetic moment.

temperature is estimated to be $T_C \simeq 13$ K from the low-field magnetization data. The Arrot plot did not enable us to determine T_C due to its strong nonlinearity. The susceptibility exhibits a discontinuous jump at $T_S \simeq 44$ K. This is ascribed to the structural transition. A similar anomaly associated with the structural transition has been found for $GaMo_4S_8$ [16]. No appreciable thermal hysteresis was found at T_S within experimental accuracy.

The inverse susceptibility shows linear temperature dependences with nearly the same Curie constant but different Weiss temperatures at $T > T_S$ and $T < T_S$. This behaviour is somewhat different from that reported in the literature [6]. The effective paramagnetic moment at $T > T_S$ is estimated to be 1.45 μ_B per formula unit, i.e. per V_4 cluster. This corresponds roughly to the magnitude expected for $S = \frac{1}{2}$ (1.73 μ_B), in accordance with an unpaired spin per V_4 cluster. An analysis, assuming an equivalent paramagnetic moment at both $T > T_S$ and $T < T_S$, gives Weiss temperatures $\theta = -15.2$ and 12.6 K for $T > T_S$ and $T < T_S$, respectively. Note that the sign is converted at T_S.

4.2. Spectrum

Since the V site in the cubic state (16e) has local trigonal symmetry, we expect, in principle, uniaxial anisotropy of the Knight shift and effects of the quadrupolar interaction at the V site. As an example of ^{51}V field-swept spectra above T_S, the result at 60 K is shown in figure 3(a). The paramagnetic spectrum was observed with a negative Knight shift. The lineshape is reproduced well by a symmetric and relatively sharp Lorentzian function, as shown by the solid curve in the figure. In other words, the anisotropy in the Knight shift and the quadrupole interaction are small and hidden in the inhomogeneous width.

Below T_S, the ^{51}V line is broadened considerably. Figure 3(b) shows the result at 17 K, which is compared with that at 60 K included in the same figure. The ^{51}V line spreads over a wide range of external field $H \simeq 5.5$ to 7.5 T. The sharp peak at $H \simeq 5.8$ T can be assigned to the signal from ^{69}Ga, because the signal from the other isotope ^{71}Ga was observed at the corresponding position. The Ga resonances have a positive Knight shift with a relatively small magnitude, which varies with temperature in proportion to the susceptibility. Although the rhombohedral distortion at T_S leads to separation of the V site, the lineshape, which can roughly

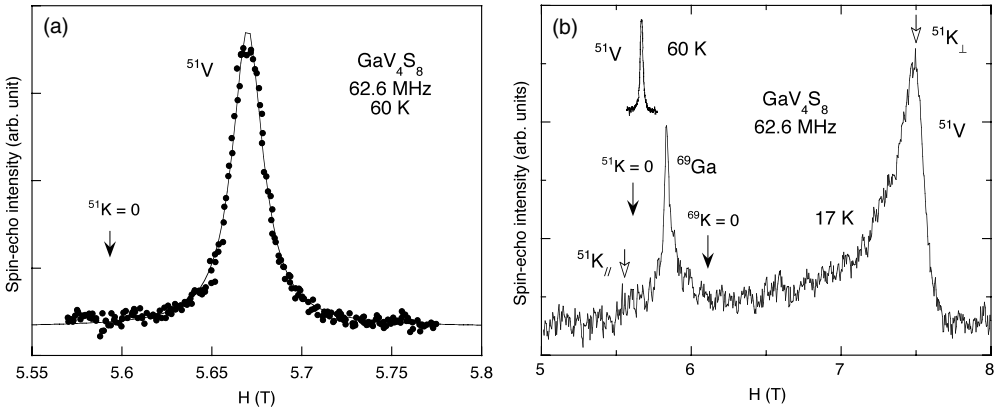

Figure 3. The field-swept NMR spectrum measured for GaV_4S_8 at 62.6 MHz, and at 60 K (a) and 17 K (b). The solid curve in (a) indicates the best-fit refinement by a Lorentzian function. The result at 60 K is also shown in (b) for comparison. Closed arrows indicate zero-Knight-shift positions. Open arrows in (b) indicate resonance fields of parallel and perpendicular components to the field.

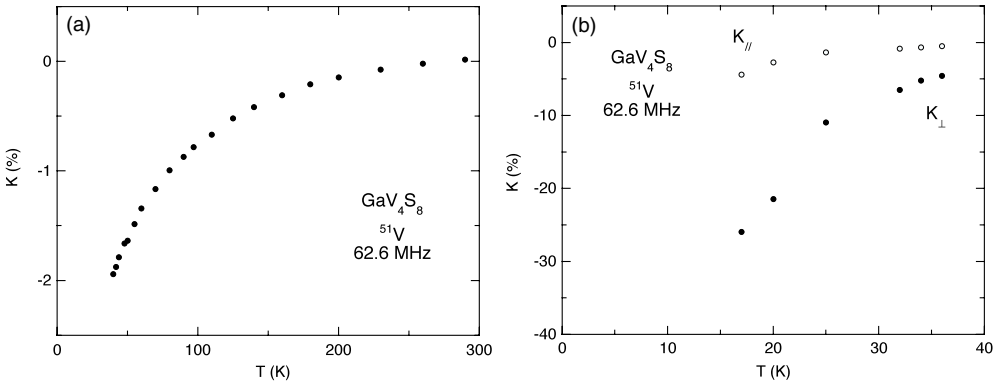

Figure 4. Temperature dependences of the ^{51}V Knight shift at $T > T_S$ (a) and $T < T_S$ (b). $K_\perp$ and $K_\parallel$ represent the components parallel and perpendicular to the field.

be reproduced by a single component of the uniaxial powder pattern, suggests that the V sites are in practically the same axial local environments. In fact, just below T_S, the lineshape could not be reproduced well by a single component of the uniaxial pattern; the structure around the peak (corresponding to the Knight-shift component perpendicular to the field $K_\perp$) is smeared, but, with decreasing temperature, turns sharp. The considerable broadening indicates an appearance of large hyperfine anisotropy below T_S.

4.3. The Knight shift

Values of the Knight shift, K, estimated from field-swept spectra measured at 62.6 MHz are shown in figures 4(a) and (b) for $T > T_S$ and $T < T_S$, respectively. Below T_S, assuming an axial Knight shift, perpendicular and parallel components to the field, $K_\perp$ and $K_\parallel$, were estimated from the peak and shoulder positions in the line, respectively. The absolute value increases with decreasing temperature, along with the increase of the susceptibility.

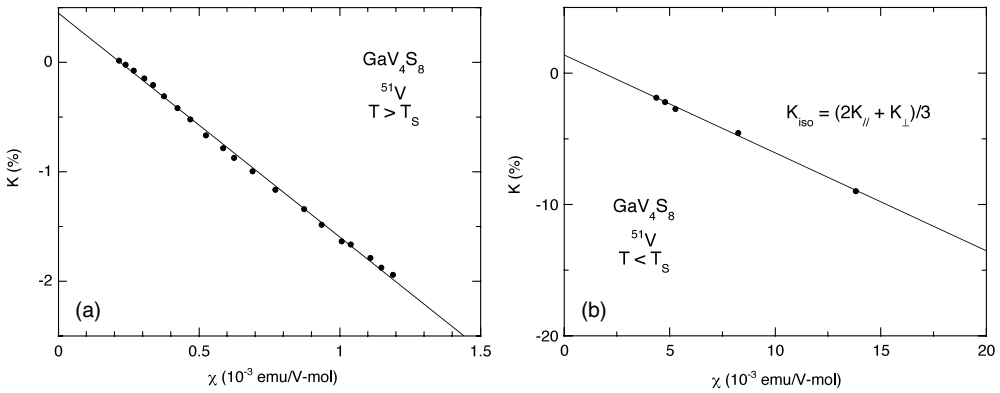

Figure 5. K–χ plots at $T > T_S$ (a) and $T < T_S$ (b). In (b), the isotropic component $K_{iso} = \frac{1}{3}(2K_\perp + K_\parallel)$ is plotted.

Figures 5(a) and (b) show K–χ plots for $T > T_S$ and $T < T_S$, respectively. The data given in figure 2 were used as the susceptibility values. In figure 5(b), the isotropic part of the Knight shift, K_{iso}, estimated from $K_{iso} = \frac{1}{3}(2K_\perp + K_\parallel)$, is plotted against the bulk susceptibility. Since the magnetization curves below 17 K were found to be nonlinear, the lower-temperature data are omitted in figure 5(b). The Knight shift in both high- and low-temperature ranges is in proportion to the susceptibility. From slopes of the fitted lines, the isotropic part of the hyperfine coupling constant, A_{iso}, is estimated to be -11.4 and $-4.2\ \mathrm{T}/\mu_B$ for $T > T_S$ and $T < T_S$, respectively. The magnitude at $T > T_S$ seems to be reasonable as a value of the isotropic component for the ^{51}V nucleus, while that at $T < T_S$ is markedly small, of approximately one third of the high-temperature value. Since we have no information on the local anisotropy in the susceptibility, it is impossible to estimate the hyperfine anisotropy. Assuming isotropy in the susceptibility, we formally derive $A_\perp = -9.9$ and $A_\parallel = -1.3\ \mathrm{T}/\mu_B$, and hence $A_{aniso} = \frac{2}{3}(A_\parallel - A_\perp) = 5.7\ \mathrm{T}/\mu_B$. Thus, the absolute value of A_{iso} is markedly reduced at T_S and, instead, large anisotropy appears. These results suggest that the intracluster electronic state is considerably modified at T_S.

4.4. Nuclear spin–lattice relaxation

The temperature dependence of the ^{51}V nuclear spin–lattice relaxation time, T_1, was measured for the paramagnetic state under external field. The operating frequency was 61.0 MHz. Below T_S, T_1 was measured at the peak position of the asymmetrically broadened spectrum. The recovery of nuclear magnetization was of single-exponential type both above and below T_S. We have not found appreciable RF-power dependence of T_1. The result for T_1 is shown in figure 6 in the form of $1/T_1T$ versus T plot. Above T_S, $1/T_1T$ decreases monotonically with temperature. A tentative fit to the Curie–Weiss-type temperature dependence, $1/T_1T = \alpha/(T - \Theta)$, reproduces the experimental data well, as shown by the solid curve in the figure. The best-fit values of α and Θ are 20 700 s^{-1} and 10.4 K, respectively. It is interesting to note that the sign of Θ is different from that of the Weiss temperature, $\theta = -15.2$ K, estimated from the susceptibility above T_S. Below T_S, $1/T_1T$ is reduced markedly. In the paramagnetic state, the spin-echo decay time T_2 was found to be nearly temperature independent with $T_2 \sim 10\ \mu$s, which is shorter than T_1 by one order.

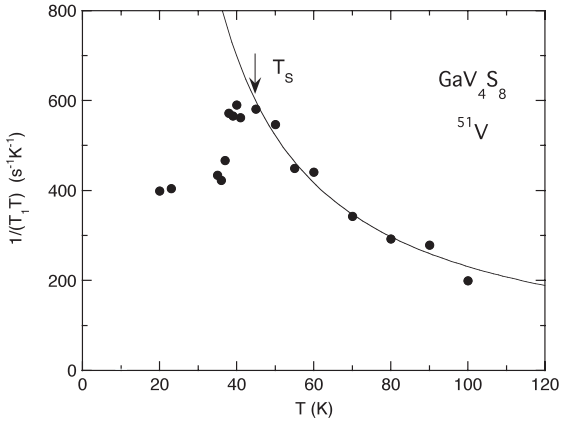

Figure 6. Temperature dependence of $1/T_1T$ above T_S measured for ^{51}V in GaV_4S_8. The solid curve indicates the best fit to the Curie–Weiss-type temperature dependence.

5. Discussion

5.1. Hyperfine interaction in the cluster compound

In this compound, each V_4 cluster is isolated well, and the interaction between clusters is probably weak. Vanadium 3d electrons are shared in the tetrahedral V_4 cluster, and each cluster behaves like a localized moment. In such a cluster, the hyperfine mechanism is not necessarily explicit. We formally divide the hyperfine field, $\boldsymbol{H}_{\rm hf}$, into intracluster and intercluster components, $\boldsymbol{H}_{\rm in}$ and $\boldsymbol{H}_{\rm out}$. Since the intercluster interaction, which is probably the classical lattice dipolar interaction, is expected to be small with respect to the intracluster coupling, we consider only $\boldsymbol{H}_{\rm in}$. In this type of cluster, $\boldsymbol{H}_{\rm in}$ should be treated as a renormalized field produced by the total spin density of cluster orbitals. However, $\boldsymbol{H}_{\rm in}$ may formally be divided into two terms: an on-site field, $\boldsymbol{H}_{\rm on}$, coming from spin density in the vicinity of the particular nucleus, and a transferred field, $\boldsymbol{H}_{\rm trans}$, added by the other three atoms inside the cluster. Hence $\boldsymbol{H}_{\rm hf}$ is summarized as $\boldsymbol{H}_{\rm hf} = \boldsymbol{H}_{\rm in} + \boldsymbol{H}_{\rm out} \simeq \boldsymbol{H}_{\rm in} = \boldsymbol{H}_{\rm on} + \boldsymbol{H}_{\rm trans}$.

In a dynamical viewpoint, if the nuclear relaxation is dominated by thermal fluctuations of exchange-coupled localized moments belonging to the clusters, namely by fluctuations of $\boldsymbol{H}_{\rm out}$, we expect temperature-independent T_1, i.e. a Curie-type temperature dependence of $1/T_1T$ [17]. Since the susceptibility analysis indicated almost the same localized moments for $T > T_S$ and $T < T_S$, we expect similar temperature dependences in both the temperature ranges. Contrary to this expectation, the experimental results show a strong reduction of $1/T_1T$ below T_S. This suggests that the ^{51}V nuclear magnetic relaxation mostly reflects the electronic state *inside* the cluster, i.e. fluctuations of $\boldsymbol{H}_{\rm in}$. For the paramagnetic state of the itinerant electron ferromagnet, $1/T_1T \propto \chi_{\rm d} \propto 1/(T - T_C)$ is expected [18], where $\chi_{\rm d}$ is the susceptibility originating from the d-band spin polarization. The experimental result is consistent with this relation. Note that the value of $\Theta = 10.4$ K, obtained from the T_1 analysis, corresponds well to $T_C \simeq 13$ K.

5.2. Origin of the structural transition

The energy scale of T_S is much larger than the magnetic interaction represented by T_C, θ and Θ, suggesting that the exchange interaction is not the principal driving force of the structural

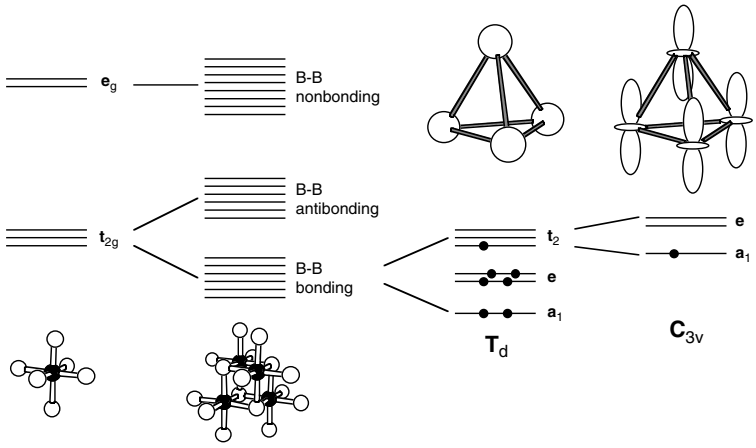

Figure 7. Qualitative 3d orbital energy level schemes of the octahedrally coordinated transition-metal atom B in BX_6 (first column) and of the B_4 cluster in B_4X_{16} consisting of four octahedrally coordinated B atoms (second column), where X represents the ligand atom like S [3]. Closed and open circles in bottom figures represent B and X atoms, respectively. The schemes in the third and fourth columns are the electron configurations expected for the V_4 cluster in cubic and rhombohedral GaV_4S_8, respectively [6]. Spin distributions in proximity to V nuclei are schematically shown for the highest occupied cluster orbitals.

transition. The reduction of the isotropic hyperfine coupling and the appearance of hyperfine anisotropy, as well as the reduction of $1/T_1T$ below T_S, point to considerable change in the electronic state inside the cluster.

The origin of the structural transition from cubic to rhombohedral has been explained reasonably by Pocha *et al* [6] based on their electronic structure calculation. Here, it may be helpful to start from a qualitative orbital scheme. Seeing the local structure around the V atom including neighbouring GaS_4 ions, the V atom is coordinated by nearly octahedral arrangement of S atoms. For a localized transition-metal atom B in an octahedral crystal field, as in BX_6, d orbitals separate into triply degenerate ground-state t_{2g} and doubly degenerate excited e_g orbitals (figure 7, first column). When four sets of BX_6 are combined to form a B_4 metal cluster, it is expected that six B–B bonding and six B–B antibonding orbitals are formed from the t_{2g} orbitals and eight B–B non-bonding orbitals from the e_g orbitals (figure 7, second column) [3]. This is because t_{2g} orbitals have electron density along B–B edges of the B_4 tetrahedron while e_g lobes orient away from the B–B bonds. The B–B bonding orbitals consist of non-degenerate a_1, doubly degenerate e and triply degenerate t_2 orbitals in the cubic symmetry (figure 7, third column) [3]. Seven 3d electrons, belonging to the $(V_4S_4)^{5+}$ cubane unit in GaV_4S_8, occupy a_1, e and t_2 orbitals in this order (at the Brillouin zone centre) [6]. This means that the triply degenerate t_2 orbitals are singly occupied, resulting in an unpaired spin per V_4 cluster. The structural transition at T_S is naturally interpreted in terms of the Jahn–Teller transition due to this cluster-orbital degeneracy. As a result of the transition, the highest orbitals separate to non-degenerate a_1 and doubly degenerate e orbitals (figure 7, fourth column), leading to partial ablation of the metallic V–V bonds. This is consistent with the reduction in the density of states in the spin excitation spectrum as observed in the T_1 measurement. This transition is of neither charge ordering nor spin localization at a certain atomic site.

The origin of the sign conversion of θ at T_S is not obvious. Probably, the macroscopic θ reflects partially the interaction *between* clusters. Since the structural deformation of the

whole lattice is small, it is difficult to explain this qualitative change by the variation in the intercluster distance and/or the bond angle. Probably the reconstruction of cluster orbitals affects the intracluster coupling as well.

It is interesting to note that the V_4 clusters, associated with localized moments, form a face-centred cubic (FCC) lattice. It is well known that the antiferromagnetic FCC system is a typical geometrically frustrated system. In this context, noting the sign conversion of θ at T_S, the spin frustration cannot be excluded as the secondary origin of the structural transition.

5.3. Origin of the large anisotropy

The large hyperfine anisotropy appears only below T_S. One of the possible origins is the anisotropy in $\boldsymbol{H}_{trans}$, which is expected to be mostly anisotropic because the intracluster atomic arrangement is asymmetric with respect to the particular atom in the cluster. The anisotropy of $\boldsymbol{H}_{trans}$, however, should be present to the same extent both above and below T_S. This is not the case. Johrendt [13] suggested for a similar compound GeV_4S_8 from calculated charge densities that the highest occupied cluster orbitals couple poorly among the neighbouring atoms. This may be the reason why the effects of $\boldsymbol{H}_{trans}$ are not appreciable.

Another possible origin is the asphericity of electron density in the immediate proximity of the particular nucleus, i.e. the anisotropy of $\boldsymbol{H}_{on}$. In the usual manner, the on-site field is divided to three contributions as $\boldsymbol{H}_{on} = \boldsymbol{H}_{Fermi} + \boldsymbol{H}_{dip} + \boldsymbol{H}_{orb}$, where $\boldsymbol{H}_{Fermi}$ is the isotropic Fermi contact field produced by the polarization of s electrons, mostly induced by unpaired 3d spins, $\boldsymbol{H}_{dip}$ the spin dipolar field originating in the asphericity of spin density distribution, and $\boldsymbol{H}_{orb}$ is the orbital field. $\boldsymbol{H}_{dip}$ is purely anisotropic and $\boldsymbol{H}_{orb}$ can also be anisotropic. Although we have no information on $\boldsymbol{H}_{orb}$, we expect a larger magnitude when the highest occupied cluster orbital is degenerate, i.e. for the state above T_S. On the other hand, $\boldsymbol{H}_{dip}$ becomes large when the spin distribution is asymmetric. Above T_S, the highest occupied t_2 cluster orbitals are triply degenerate. In this case, the local spin density in proximity to the nucleus is like the mixed state of three orbitals with d_{xy}-, d_{yz}- and d_{zx}-type spatial distribution, which results in a spherical spin density as schematically shown in figure 7. On the other hand, the occupation of the a_1 orbital, consisting purely of the d_{z^2} contribution [6] as also shown in figure 7, explains the appearance of the large anisotropy below T_S. From a crystallographic viewpoint, the V site separates into two inequivalent sites below T_S. The ^{51}V NMR spectrum below T_S, however, involves a practically single component. This is reasonable because the spectral shape is mostly determined by $\boldsymbol{H}_{in}$ and the spin density in the proximity of nuclei is equivalent at all the V sites, even below T_S.

On the other hand, the isotropic term of hyperfine coupling is usually ascribed to the polarization of core electrons induced by exchange interaction with d electrons. The origin of the reduction in A_{iso} at T_S may not be straightforward. Quantitative information on the mixing between core electrons and d orbitals at each state seems to be necessary.

6. Concluding remarks

GaV_4S_8 includes tetrahedral V_4 clusters coupled weakly with each other. Each V_4 cluster behaves like a localized moment with nearly $S = \frac{1}{2}$. Metallic V–V bonds are expected within the cluster. This compound shows a structural transition at $T_S \simeq 44$ K and a ferromagnetic ordering at $T_C \simeq 13$ K. The macroscopic magnetic interaction changes the sign at T_S. In this study, the structural transition was investigated microscopically by means of ^{51}V NMR. The experimental results are summarized as follows. (1) Below T_S, the isotropic term of ^{51}V hyperfine coupling is reduced markedly, and instead, large anisotropy appears. (2) The

relaxation rate, $1/T_1$, is markedly reduced below T_S, suggesting considerable reduction of the density of states in the spin excitation spectrum below T_S. Both of these indicate that the electronic state *inside* the cluster is markedly modified at T_S. The structural transition can be interpreted as the Jahn–Teller effect driven by the cluster-orbital degeneracy of the highest occupied 3d-based orbitals. The drastic change in the NMR quantities at T_S can be explained well in terms of the cluster orbital schemes [6]; the unpaired 3d electron occupies nearly spherical degenerate cluster orbitals at $T > T_S$, and an asymmetric non-degenerate one at $T < T_S$. Some of the structural anomalies found in pyrochlore compounds may be ascribed to this type of local instability inherent to the tetrahedral structure.

Acknowledgments

The authors acknowledge Professor K Yoshimura for valuable discussions. This work was supported by Grants-in-Aid for Scientific Research from the Ministry of Education, Culture, Sports, Science and Technology, Japan.

References

[1] For a review, see for example, Imada M, Fujimori A and Tokura Y 1998 *Rev. Mod. Phys.* **70** 1039
[2] For a review, see for example, Moessner R 2001 *Can. J. Phys.* **79** 1283
[3] Harris S 1989 *Polyhedron* **8** 2843
[4] Rastogi A K 1987 *Current Trends in the Physics of Materials* (Singapore: World Scientific) p 316
[5] Brasen D, Vandenberg J M, Robbins M, Willens R H, Reed W A, Sherwood R C and Pinder X J 1975 *J. Solid State Chem.* **13** 298
[6] Pocha R, Johrendt D and Pöttgen R 2000 *Chem. Mater.* **12** 2882
[7] Vandenberg J M and Brasen D 1975 *J. Solid State Chem.* **14** 203
[8] Sahoo Y and Rastogi A K 1993 *J. Phys.: Condens. Matter* **5** 5953
[9] Sahoo Y and Rastogi A K 1995 *Physica* B **215** 233
[10] Sahoo Y and Rastogi A K 1996 *J. Phys. Chem. Solids* **57** 467
[11] Rastogi A K and Niazi A 1996 *Physica* B **223/224** 588
[12] Shanthi N and Sarma D D 1999 *J. Solid State Chem.* **148** 143
[13] Johrendt D 1998 *Z. Anorg. Allg. Chem.* **624** 952
[14] Barz H 1973 *Mater. Res. Bull.* **8** 983
[15] Fransois M, Lengauer W, Yvon K, Ben Yaich-Aerrache H, Gougeon P, Potel M and Sergent M 1991 *Z. Kristallogr.* **196** 111
[16] Shamrai V, Mädge H, Mydlarz T and Leitus G 1982 *J. Low Temp. Phys.* **49** 123
[17] Moriya T 1956 *Prog. Theor. Phys.* **16** 641
[18] Moriya T and Ueda K 1974 *Solid State Commun.* **15** 169